

Review

# On the Durability and Wear Resistance of Transparent Superhydrophobic Coatings

Ilker S. Bayer

Smart Materials, Istituto Italiano di Tecnologia, Via Morego 30, 16163 Genoa, Italy; ilker.bayer@iit.it;  
Tel.: +39-380-387-6699

Academic Editor: Mariateresa Lettieri

Received: 24 November 2016; Accepted: 9 January 2017; Published: 18 January 2017

**Abstract:** Transparent liquid repellent coatings with exceptional wear and abrasion resistance are very demanding to fabricate. The most important reason for this is the fact that majority of the transparent liquid repellent coatings have so far been fabricated by nanoparticle assembly on surfaces in the form of films. These films or coatings demonstrate relatively poor substrate adhesion and rubbing induced wear resistance compared to polymer-based transparent hydrophobic coatings. However, recent advances reported in the literature indicate that considerable progress has now been made towards formulating and applying transparent, hydrophobic and even oleophobic coatings onto various substrates which can withstand certain degree of mechanical abrasion. This is considered to be very promising for anti-graffiti coatings or treatments since they require resistance to wear abrasion. Therefore, this review intends to highlight the state-of-the-art on materials and techniques that are used to fabricate wear resistant liquid repellent transparent coatings so that researchers can assess various aptitudes and limitations related to translating some of these technologies to large scale stain repellent outdoor applications.

**Keywords:** transparent superhydrophobic; oleophobic; wear abrasion; hydrophobic nanoparticles; anti-graffiti coatings

---

## 1. Introduction

One of the most challenging aspects of preparing non-wettable coatings is to maintain a good degree of transparency while retaining robust and scratch resistant self-cleaning and stain free characteristics [1–3]. Transparency and surface roughness are generally contradictory properties. Hydrophobicity of low surface energy coatings increases with surface roughness but coating transparency often decreases because of Mie scattering from the rough surface. When the roughness dimension is much smaller than the light wavelength, the film/coating becomes increasingly transparent due to refractive index change between air and the coating, which effectively reduces the intensity of refraction at the air (or water)/film interface and increases the optical quality. In other words, it is necessary to control the roughness below 100 nm to effectively lower the intensity of Mie scattering while maintaining non-wettable characteristics [4].

A forthright large-scale application of transparent non-wetting coatings is the prevention of unwanted markings in public areas or on public transportation vehicles known as graffiti. Graffiti prevention (anti-graffiti) treatments can be in the form of (a) transparent and self-adherent polymer films that can be peeled off and replaced from time to time; (b) in the form of polymeric paints (non-sacrificial) that are able to repel stains and graffiti tagging; or (c) they can be stain and dust repellent coatings obtained from ceramic precursors particularly suitable for special applications such as solar panels [5,6]. It is also important to take into account how the graffiti is applied. Most of the commercially available anti-graffiti paints are siloxane/silicone-based formulations and they can repel a majority of water-based paints and markers. However, if the graffiti is applied from a solvent or

oil based paint, silicone chemistry may not protect against graffiti tagging due to solid surface energy and liquid surface tension match between the siloxane polymers and oil-based paint vehicle [7,8]. In other words, the coating should practically be oleophobic or superomniphobic in order to repel oil-based paints. Although beyond the scope of this review, another important aspect to consider is the type of the surface on which permanent marks (unwanted staining) are induced. In other words, a window like smooth transparent surface or highly porous concrete, brick, limestone, slate, wood and masonry walls. For instance, due to the high porosity of such surfaces, the graffiti is absorbed into the texture to a substantial degree, thereby making it difficult to remove or clean compared to smooth non-porous surfaces.

Mechanical robustness of non-wettable coatings signifies their resistance to wear as a result of rubbing induced abrasion [9,10]. In general, there are two approaches to creating a durable nonwetting surface: (a) limiting material removal so as to retain superhydrophobicity under wear for as long as possible and (b) developing a material that maintains superhydrophobicity as it wears away. For the latter type, such performance for surfaces under a single wear condition is known as “wear similarity”. A simple example of wear similarity is sanded Teflon (polytetrafluoroethylene, PTFE) which can be rendered superhydrophobic by using fine grit sandpaper so that continued sanding would retain superhydrophobicity until the Teflon material is completely worn away. In almost all the cases reported in the literature, the most durable non-wettable surfaces or coatings that can withstand the abovementioned approaches are polymer-based nanocomposites [11,12]. However, recent progress indicates that transparent non-wettable coatings can also be produced with reasonable robustness, which can eventually resist continuous harsh abrasion conditions by one of the two abovementioned mechanisms.

In this review, article, we will distinctly analyze state-of-the-art on various transparent non-wetting coatings and treatments except for the sacrificial transparent films. We will review fabrication aspects of transparent nanoparticle films and coatings and ways to render them resilient against abrasion induced wear. Next, we will present and discuss transparent, flexible and non-wettable materials obtained by various mold transfer processes including nanoimprint lithography which utilize hydrophobic transparent elastomer precursors or others with UV-induced polymerization. Finally, we will present fabrication aspects and characteristics of ceramic precursor based transparent non-wettable coatings that are deemed suitable for windows or solar energy conversion unit surfaces. In each category, we will address inherent limitations, potentials for immediate outdoor applicability and future directions in order to render such transparent non-wetting coatings more resilient against wear abrasion.

## 2. Wetting Theories, Surface Roughness and Robust Metastable Superhydrophobicity

The most customary superhydrophobic surface roughness model is that of lotus leaf. On its surface both microscale and nanoscale protruding structures are found. It has been understood that in fact many plant leaves do not possess low-energy surface compounds that are commonplace in the fabrication of synthetic non-wettable materials. The most hydrophobic constituent is the epicuticular wax, and the apparent contact angle of water on waxes is only slightly above 90°, which is certainly not sufficient to explain extreme non-wettability on certain plant surfaces. Herminghaus [13] also showed that it is possible to maintain non-wettability when instead of a protruding micro/nano texture, closed pore-like micro/nano texture is present even though hydrophobic chemistry is associated with the wetting of wax surface.

In its most simplistic form, wetting and surface roughness are correlated with two theories known as Wenzel and Cassie-Baxter [14]. As described by Marmur [14], wetting on rough surfaces may assume either of two regimes: homogeneous wetting (corresponding to Wenzel theory of hydrophobicity), where the liquid completely penetrates the roughness grooves, or heterogeneous wetting (corresponding to Cassie-Baxter theory of superhydrophobicity), where air (or another fluid) is trapped underneath the liquid inside the roughness grooves. In a way, durability or “robustness” of a superhydrophobic surface relies on how long it can resist the transition between these regimes [15].

In other words, metastable states (minimum liquid-solid contact) in which minimum droplet-surface contact points are maintained, have to be long lived. Evolution of non-wetting surfaces in nature also followed this approach as shown by calculations [14]. This strategy avoids the need for high steepness protrusions that may be more prone to erosion, wear and breakage. In addition, due also to the specific shape of the Lotus leaf protrusions, this strategy lowers the sensitivity of the superhydrophobic state to the protrusion distance.

As such, the complex relationship between surface roughness and durable superhydrophobicity can be summarized as follows:

- Microscale roughness features should resist damage under abrasion induced wear [10];
- Deeply embedded nanoscale features (away from the exposed microscale protrusions) can ensure longer superhydrophobic resistance against wear abrasion [16];
- A self-similar hierarchical texture throughout the non-wettable surface, film or coating bulk should be constructed in order to resist material removal due to wear abrasion [9];
- From tribology standpoint, energy or stress dissipating ceramic nanoparticles or organics should be built-in to the coatings such as rubbery domains [17].

Coating surface mechanical durability requires resistance to smoothing out in two roughness scales [16]. Once transparency is also introduced into the equation, resistance to durability becomes more problematic since transparent surface texture roughness should not enhance Mie and Rayleigh scattering [18]. Mie scattering occurs when the diameter of the surface features are close to the wavelength of the incident photon, and Rayleigh scattering occurs when the size of the surface features are much smaller than the wavelength of the incident photon. Note that herein we define “contact angle” as the apparent contact angle that is stable over time on a surface. In other words, the apparent contact angle on a superhydrophobic surface can still be greater than  $150^\circ$  but the droplet would not roll off or slide over the coating when tilted. On such surfaces, the real contact angle is established at submicron scales along the contact line, known as *sticky* superhydrophobicity.

### 3. Wear Damage Resistance Characterization Methods

Since recent reviews have sufficiently covered measurement and characterization of wear durability of non-wettable surfaces [10], it would be abundant to repeat them herein. However, some clarifications are needed in order to discuss “robustness” of non-wettable surfaces properly. Mechanical durability of non-wettable coatings is a broad terminology. It is used if the non-wettable surface is for instance stretch or bending resistant but also for abrasion induced wear. Some non-wettable coatings that were not properly tested against abrasion induced wear have been classified as durable if they showed good substrate adhesion [19]. Therefore, it is imperative to explicitly indicate the type of “robustness” the coating demonstrates or is tested against. For instance, there are many experimental tests that a non-wettable surface should pass in order to be classified as “robust” or mechanically durable that can be acceptable from an industrial application point of view. For instance, peel tests for substrate adhesion (including water immersion related lift off), underwater ultrasonic processing, both sand and rain (spray) based erosion damage, bending and flexibility, high pressure hydrostatic liquid build-up, scratch resistance and abrasion induced wear.

Of course, at the end of all these tests, the ideal Cassie-Baxter non-wetting state should prevail. In other words, droplets should freely roll off (not slide) the surfaces. In certain cases, due to wear abrasion, the non-wettable surface can transform into a superhydrophobic state but with low droplet mobility (high substrate tilt angles for droplet motion), generally referred to as rose petal effect [20,21], even though the hierarchical surface texture is preserved. This can still be considered as resistance to abrasion induced wear if the surface of the coating can be transformed back into a non-stick superhydrophobic state by a simple post treatment such as thermal annealing or a thin silane coating etc. [22].

In this review, we will focus on coating resistance against abrasion induced wear on transparent non-wettable coatings. It is believed that wear abrasion is the most relevant durability parameter that can be convincing for potential industrial applications as well as for outdoor anti-graffiti installations. Wear abrasion of transparent non-wettable coatings has not been adequately addressed so far and more R&D efforts are needed in order to allow commercialization.

#### 4. Transparent Non-Wettable Coatings from Nanoparticle Assembly

Rahmawan et al. [23] reviewed and discussed different self-assembly methods, including sol-gel processes, micro-phase separation, templating, and nanoparticle assembly, to create transparent, superhydrophobic surfaces. The review of literature indicates that one of the most commonly used nanoparticles in the fabrication of non-wettable coatings is SiO<sub>2</sub> nanoparticles [24]. They are extensively used in super-repellent polymer nanocomposite coatings but also in the fabrication of transparent non-wettable coatings. Irzh et al. [25] described a novel one-step or two short-step method for the production of superhydrophobic SiO<sub>2</sub> layers using microwave plasma. The one-step reaction was applied for the production of a transparent superhydrophobic layer that was not very UV-stable or a superhydrophobic UV-stable layer that was not very transparent. The two-step method but short process was applied for the production of a superhydrophobic transparent and UV-stable SiO<sub>2</sub> layer. Only a few seconds were required to produce these layers via a plasma polymerization mechanism. The authors used TEOS (silane-SiO<sub>2</sub> precursor) for roughness, decane (hydrocarbon precursor), perfluorodecaline (C<sub>10</sub>F<sub>18</sub>) or perfluorononane (C<sub>9</sub>F<sub>20</sub>) (fluorocarbon precursors). The microwave plasma reactor was loaded with the silica precursor and any one of the organic hydrophobic precursors to form a rough SiO<sub>2</sub> nanostructured surface functionalized with waxy or fluorinated macromolecules. Although the authors used many different substrates for deposition they did not report any performance related to mechanical abrasion resistance of the layers.

Bravo et al. [26] utilized the layer-by-layer assembly method to control the placement and level of aggregation of differently sized SiO<sub>2</sub> nanoparticles within the resultant multilayer thin film. They fully exploited the advantages of layer-by-layer processing to optimize the level of roughness needed to obtain superhydrophobicity and a low contact angle hysteresis and at the same time minimize light scattering (Figure 1a). Besides high transmittance (Figure 1b) and superhydrophobicity, very low levels of reflectivity was also achieved at specified visible wavelengths.

They created transparent superhydrophobic films by the sequential adsorption of silica nanoparticles and poly(allylamine hydrochloride). The final assembly was rendered superhydrophobic with silane treatment. Optical transmission levels above 90% throughout most of the visible region of the spectrum were realized in optimized coatings. Advancing water droplet contact angles as high as 160° with low contact angle hysteresis (<10°) were obtained for the optimized multilayer thin films. Because of the low refractive index of the resultant porous multilayer films, they also exhibited antireflection properties.

Wong and Yu [27] reported a simple protocol to prepare superhydrophobic and hydrophobic glass by treating standard microscope slides with methyltrichlorosilane and octadecyltrichlorosilane, respectively as shown in Figure 2a. Octadecyltrichlorosilane formed a closely packed, methyl-terminated, self-assembled monolayer that changed the glass surface from hydrophilic to hydrophobic (Figure 2b). Treatment with methyltrichlorosilane resulted in 3-dimensional polymethylsiloxane networked nanostructures, which produced a superhydrophobic surface. In both cases, the glass slides maintained optical transparency despite remarkable changes in the surface wettability (Figure 2a).

Tuvshindorj et al. [3] investigated the effect of different levels of surface topography on the stability of the Cassie state of wetting (droplets freely roll off the surfaces) in large-area and transparent superhydrophobic coatings. Three different organically modified silica (ormosil) coatings, (i) nanoporous hydrophobic coating (NC); (ii) microporous superhydrophobic coating (MC); and (iii) double-layer superhydrophobic coating with nanoporous bottom and microporous top layers (MNC), were prepared on glass surfaces (Figure 3a). The stability of the Cassie state of coatings against the

external pressure was examined by applying compression/relaxation cycles to water droplets sitting on the surfaces (Figure 3b).

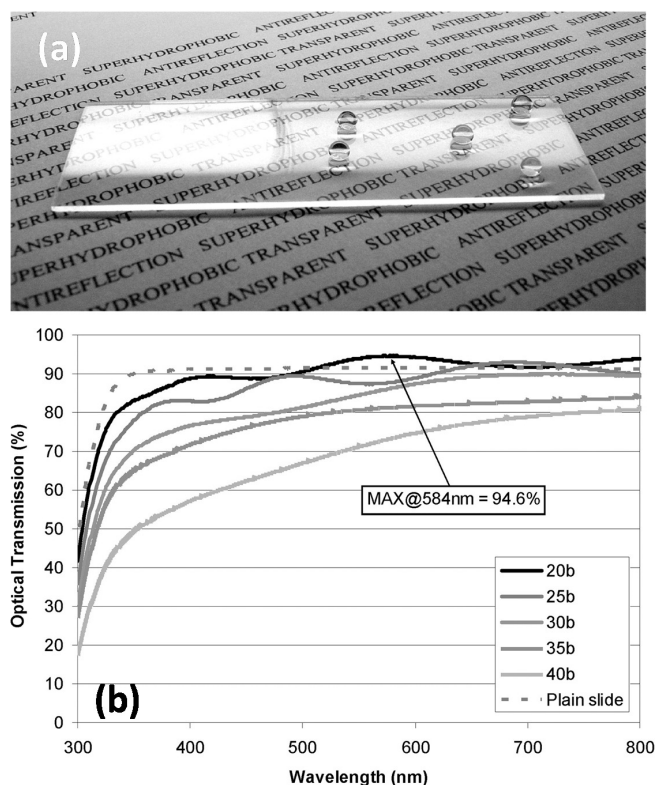


**Figure 1.** (a) Photograph of a glass slide coated with a transparent, superhydrophobic multilayer with antireflection properties: [PAH (7.5)/(50 + 20 nm) SiO<sub>2</sub> (9.0)] 20 + top-layers film. The right side of the glass slide is coated with the multilayers; (b) Transmittance of multilayer films with 20 to 40 bilayers of [PAH (7.5)/(50 + 20 nm) SiO<sub>2</sub> (9.0)] × and top layers. The transmittance of a plain glass slide (substrate for the films) is also plotted [26].

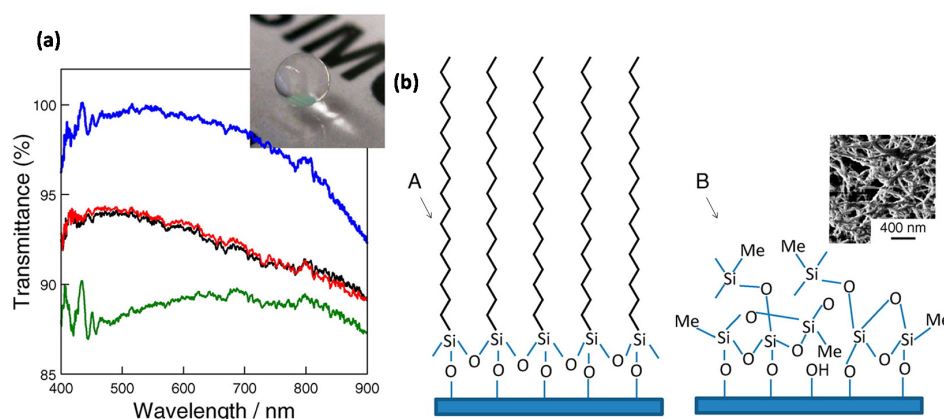


**Figure 2.** (a) UV-Vis spectra showing the transmittance of glass slides: untreated (black trace); hydrophobic (red line); superhydrophobic prepared at room temperature (green line); superhydrophobic glass prepared at 4 °C (blue line). The inset image shows a water droplet on a transparent superhydrophobic slide; (b) Schematic representation of a normal hydrophilic glass surface after treatment with (A) octadecyltrichlorosilane that results in the formation of a highly ordered self-assembled monolayer (hydrophobic) and (B) methyltrichlorosilane that results in the formation of a 3D polymethylsiloxane network (superhydrophobic). The inset shows a SEM image of the superhydrophobic surface [27].

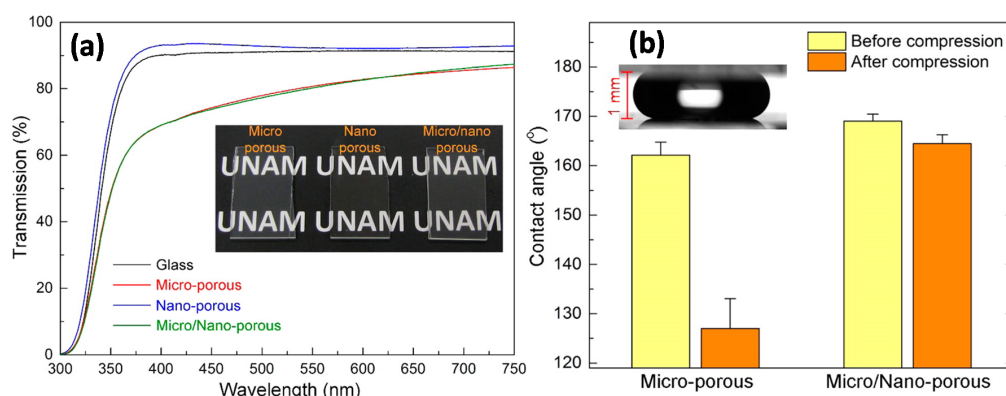


**Figure 3.** (a) Transmission spectra of ormosil coatings and an uncoated glass substrate. All of the coatings are highly transparent at the visible wavelengths. The inset shows a photograph of transparent coatings; (b) Droplet squeezing between two identical surfaces. Contact angles of surfaces before and after compression. The inset shows the squeezed water droplet between two MNC surfaces. There is only a slight decrease in the contact angle of the MNC after compression. The large decrease in the MC shows loss of the superhydrophobic property [3].

The changes of the apparent contact angle, contact-angle hysteresis, and sliding-angle values of the surfaces before and after compression cycles were studied to determine the Cassie/Wenzel transition behavior of the surfaces. In addition, water droplets were allowed to evaporate from the surfaces under ambient conditions, and the changes in the contact angles and contact-line diameters with increasing Laplace pressure were analyzed. They showed that, upon combination of coatings with different levels of topography it was possible to fabricate transparent superhydrophobic surfaces with extremely stable Cassie-Baxter states of wetting on glass surfaces. The stability of the Cassie state (droplets freely roll away) of the coatings against the external pressure was investigated. It was observed that a droplet sitting on a single-layer coating can easily transform to a sticky Wenzel state (hydrophobic but droplets can no longer roll away or slide over the surface) from a roll-off Cassie state under external pressures as low as approximately 80 Pa. On the other hand, Cassie to Wenzel state transition was observed at around 1600 Pa for a double-layer micro/nanoporous coating, which is almost 4-fold higher than the transition pressure for a Lotus leaf (slightly above 400 Pa). The extreme stability of the Cassie-Baxter state in a micro/nanoporous coating was attributed to its double-layer porous structure. With increasing external pressure, the contact line of a droplet in the Cassie-Baxter state gradually slipped down from the walls of a microporous top layer, and after a critical pressure, the contact line touched the nanoporous bottom layer. After removal of the pressure, the contact line partially recovered in the sense that dewetting of the nanoporous bottom layer took place. Although not indicated by the authors explicitly, this recovery was possibly an intermediate wetting state [28]. The authors did not report on the resilience of such coatings against abrasion or other similar means of wear effect.

Xu et al. [29] studied the non-wettable properties and transparency of coatings made from the assembly of fluorosilane modified silica nanoparticles (F-SiO<sub>2</sub> NPs) via one-step spin-coating and dip-coating without any surface post-passivation steps as shown in Figure 4. When spin-coating the hydrophobic NPs (100 nm in diameter) at a concentration  $\geq 0.8$  wt.% in a fluorinated solvent, the surface exhibited superhydrophobicity with an advancing water contact angle greater than 150° and a water droplet (5  $\mu$ L) roll-off angle less than 5°. In comparison, superhydrophobicity was not achieved by dip-coating the same hydrophobic NPs. Scanning electron microscopy (SEM) and atomic force microscopy (AFM) images revealed that NPs formed a nearly close-packed assembly in the superhydrophobic films, which effectively minimized the exposure of the underlying substrate while offering sufficiently trapped air pockets (Figure 4c,d). In the dip-coated films, however, the surface coverage was rather random and incomplete (Figure 4a,b).

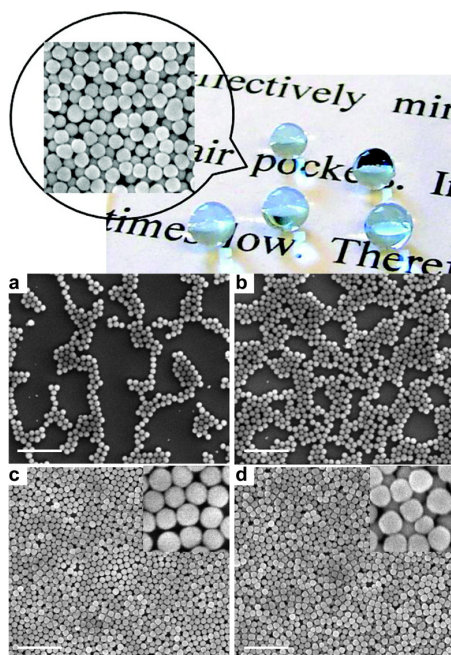


**Figure 4.** Top Panel: Photograph of the transparent F-SiO<sub>2</sub> NP (fluorinated silica nanoparticle film) on a glass slide. SEM images of spin-coated 100 nm F-SiO<sub>2</sub> NPs with different concentrations on TESPSA-functionalized Si wafers: (a) 0.1, (b) 0.4, (c) 0.8, and (d) 1.2 wt.%. The insets in c and d are high-magnification images. Scale bars: 1 μm [29].

Therefore, the underlying substrate was exposed and water was able to impregnate between the NPs, leading to smaller water contact angle and larger water contact angle hysteresis. The spin-coated superhydrophobic film was also highly transparent with greater than 95% transmittance in the visible region. They demonstrated that the one-step coating strategy could be extended to different polymeric substrates, including poly(methyl methacrylate) and polyester fabrics, to achieve superhydrophobicity [29].

Xu and He [30] described a simple and effective method to fabricate transparent superhydrophobic coatings using 3-aminopropyltriethoxysilane (APTS)-modified hollow silica nanoparticle sols. The sols were dip-coated on slide glasses, followed by thermal annealing and chemical vapor deposition with 1*H*,1*H*,2*H*,2*H*-perfluorooctyltrimethoxysilane (POTS). The largest water contact angle (WCA) of coating reached as high as 156° with a sliding angle (SA) of ≤2° and a maximum transmittance of 83.7%. The highest transmittance of coated slide glass reached as high as 92% with a WCA of 146° and an SA of ≤6°. A coating simultaneously showing both good transparency (90.2%) and superhydrophobicity (WCA: 150°, SA: 4°) was achieved through regulating the concentration of APTS and the withdrawing speed of dip-coating. Scanning electron microscopy (SEM), transmission electron microscopy (TEM), and atomic force microscopy (AFM) were used to observe the morphology and structure of nanoparticles and coating surfaces. Optical properties were characterized by a UV-visible spectrophotometer. Surface wettability was studied by a contact angle/interface system. The effects of APTS concentration and the withdrawing speed of dip-coating were also discussed on the basis of experimental observations. They did not perform any abrasion induced wear-resistance experiments on the transparent non-wettable coatings.

Zhu et al. [31] produced a transparent superamphiphobic coating using carbon nanotubes (CNTs) as a template as shown in Figure 5a–f. The optical transmittance of the resulting coating was greater than 80% throughout a broad spectrum of ultraviolet and visible wavelengths. Meanwhile, water and numbers of extremely low surface tension liquids, such as dodecane (25.3 mN/m), did not wet the coatings and could roll off easily (Figure 5g). They did not report any abrasion induced wear-resistance

properties of the coatings but the superamphiphobic property of the obtained transparent coating was kept even after thermal treatment at 400 °C. Separate experiments demonstrated that CNTs-directed surface texture enhanced the oleophobicity significantly by promoting high CA and low CAH with liquids tested, when compared to the pure SiO<sub>2</sub>- and carbon black-directed surface texture.

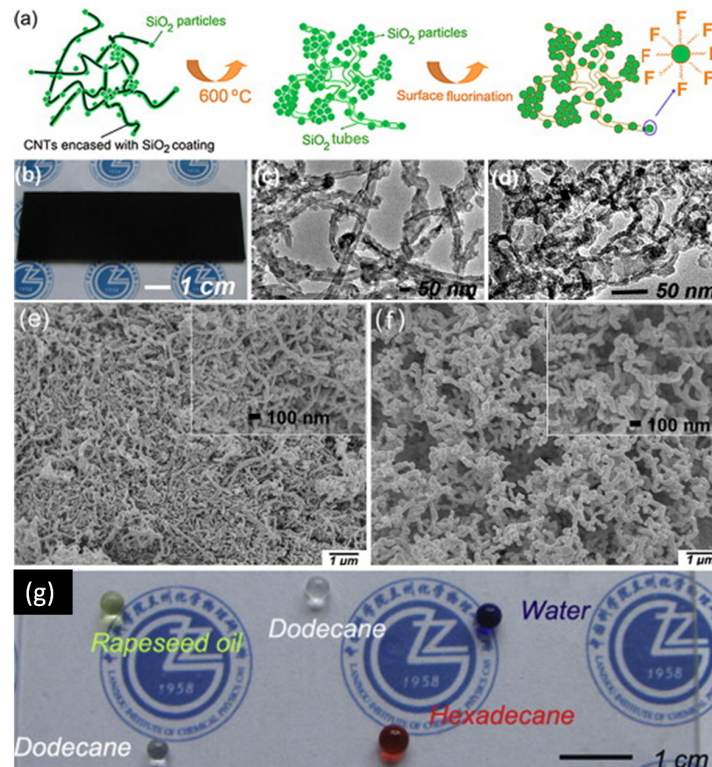


**Figure 5.** (a) Schematic diagram illustrating the fabrication procedure of the transparent superamphiphobic coating; (b) digital image of the CNTs–SiO<sub>2</sub> coating sprayed onto glass slide; TEM images of the sprayed CNTs–SiO<sub>2</sub> coating before (c) and after (d) thermal treatment; FESEM images of the sprayed CNTs–SiO<sub>2</sub> coating before (e) and after (f) thermal treatment; (g) transparent state of the coating after thermal treatment to burn away the CNTs. Various liquid droplets are also visible in their non-wetting state [31].

Ling et al. [32] produced a superhydrophobic surface with a static water contact angle WCA > 150° using a simple dip-coating method of 60-nm SiO<sub>2</sub> nanoparticles onto an amine-terminated (NH<sub>2</sub>) self-assembled monolayer (SAM) glass/silicon oxide substrate, followed by chemical vapor deposition of a fluorinated adsorbate (Figure 6). For comparison, they also fabricated a close-packed nanoparticle film, formed by convective assembly, which gave WCA ~ 120°. The mechanical stability (adhesion to substrate) of the superhydrophobic coating was enhanced by sintering of the nanoparticles in an O<sub>2</sub> environment at high temperature (1100 °C). A sliding angle of < 5° indicated the self-cleaning properties of the surface. The dip-coating method was applied to glass substrates to prepare surfaces that are superhydrophobic and transparent. They indicated that for potential commercial application of a self-cleaning superhydrophobic surface, the mechanical integrity of the nanoparticle film must be sufficient to withstand wear. However, they tested their surfaces using a standard tape peel test rather than a real wear abrasion test. Adhesive tape with a pressure-sensitive adhesive (PSA) was applied on the surface and removed from the surface prior to gas phase deposition of 1H,1H,2H,2H-perfluorodecyltriethoxysilane (PFTS) because PFTS prevents the adhesion of scotch tape on the surface. The nanoparticle films before and after the peel tests were examined by SEM (Figure 6A,B).

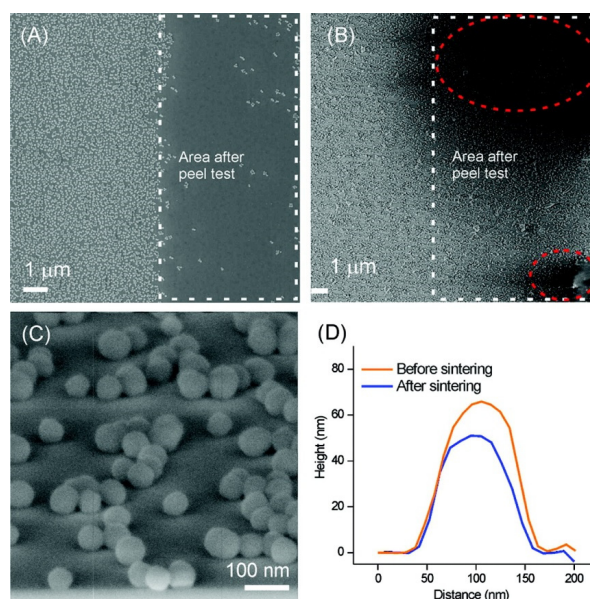
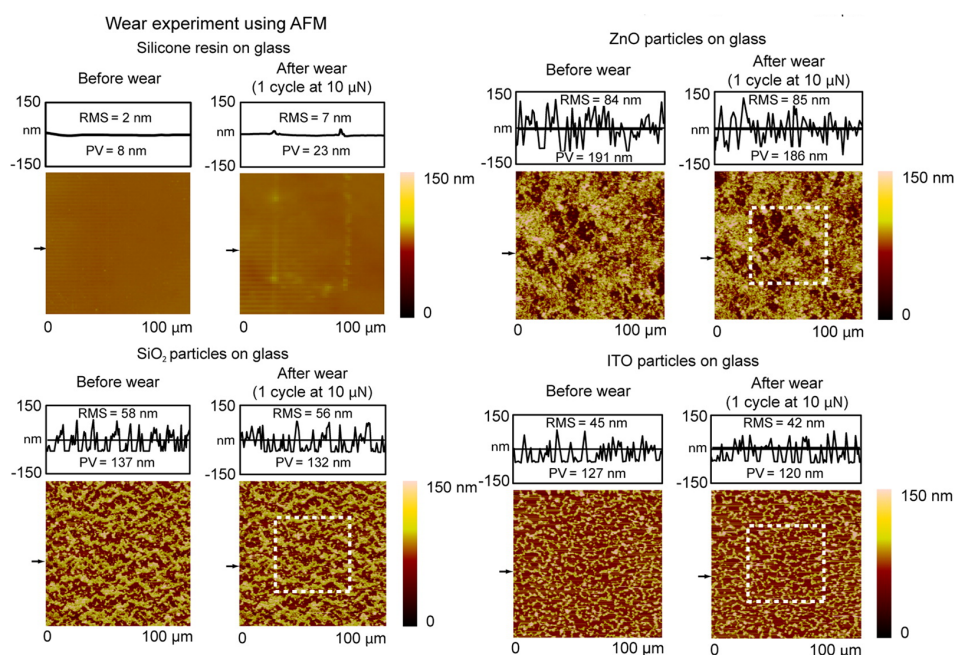


**Figure 6.** SEM images of the peel test on dip-coated nanoparticle films before (A) and after a sintering process (B); white boxes indicate the areas after peel tests, while red-dot ellipsoids show the area where scotch tape adhesives remained on the substrate after the test; (C) Titled SEM image of the nanoparticles after sintering, and (D) averaged height profiles of the nanoparticles before and after sintering (as measured by AFM) [32].

Figure 6A shows such nanoparticle film after the peel test. In the area highlighted by the white square, where the peel test was applied, almost all the nanoparticles were removed from the surface, indicating a rather poor adhesion of the nanoparticles on the  $\text{NH}_2$ -SAM. In order to improve the stability and to obtain a stable superhydrophobic surface, the substrates were subjected to a sintering process at high temperature. Sintering was performed under  $\text{O}_2$  at  $1100\text{ }^\circ\text{C}$  for 2 h. Figure 6B shows the SEM image of the as-sintered substrate after the peel test. The areas with and without peel test showed an equally dense coverage of nanoparticles, indicating a good stability of the nanoparticle layer. This is attributed to the chemical and thermal bonding of nanoparticle onto the  $\text{SiO}_2$  substrates. Some tape adhesives were seen on top of the nanoparticles (red ellipsoids in Figure 6B), which refers to a partial adhesive failure between the PSA and the sintered and hydrophilic surface. Lowering the sintering time to 30 min and the sintering temperature to  $900$  or  $1000\text{ }^\circ\text{C}$  was possible without apparent loss of adhesion improvement. After deposition of PFTS, the static water contact angle was  $150^\circ$ , indicating the formation of a stable superhydrophobic surface on the sintered substrate. After sintering at  $1100\text{ }^\circ\text{C}$  for 30 min, the nanoparticles were only slightly melted onto the substrates (Figure 6C). No obvious deformation was observed. The height profiles of 20 nanoparticles were averaged on samples before and after sintering (Figure 6D), showing that the aspect ratios (height/fwhm) of the nanoparticles before and after sintering were 1.1 and 0.9, respectively.

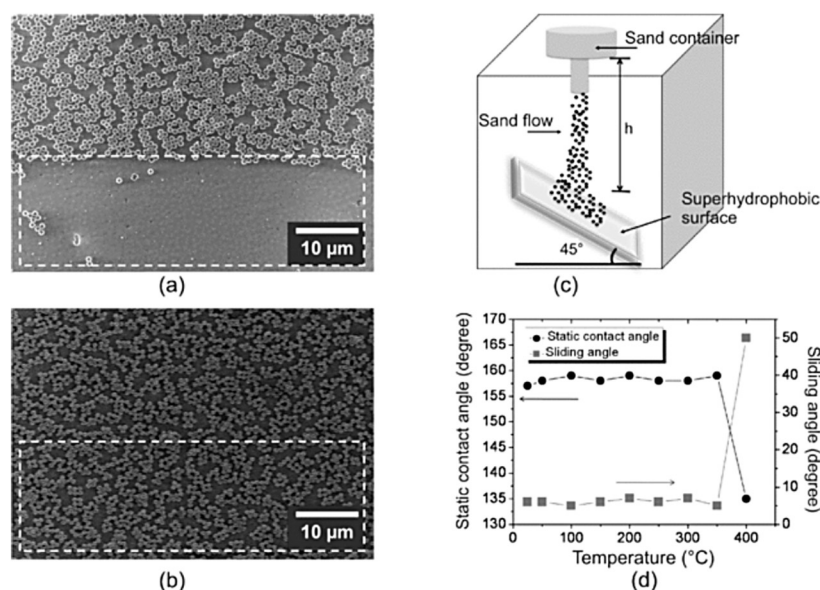
Ebert and Bhushan [33] performed a systematic study in which transparent superhydrophobic surfaces were created on glass, polycarbonate, and poly(methyl methacrylate) (PMMA) substrates using surface-functionalized  $\text{SiO}_2$ , ZnO, and indium tin oxide (ITO) nanoparticles. The contact angle, contact angle hysteresis, and optical transmittance were measured for samples using all particle-substrate combinations. To examine wear resistance, multiscale wear experiments were performed using an atomic force microscope (AFM) and a water jet apparatus. Dip coating was used as the means of fabrication. They used commercial and silane-modified  $\text{SiO}_2$  nanoparticles as well as ZnO and ITO particles which were not surface-modified and used as received. To hydrophobize them, they were treated in solution by octadecylphosphonic acid (ODP) and the prepared samples did not require post-treatment with low surface energy substances.

Figure 7 shows the AFM induced wear results on coatings deposited on glass. Changes in roughness due to wear are given as roughness profile above each AFM topography panel. The nanoparticles showed different tendencies in the way they deposited onto substrates from dip coating, which was attributed to differences in primary particle size. This caused variation in coating thickness and morphology between particles, which was reflected as differences in wettability and transmittance between samples. ITO samples had slightly lower WCA and slightly higher CAH than  $\text{SiO}_2$ , ZnO, which is likely the result of a comparatively lower liquid-air fractional area. Roughness and coating thickness influenced transmittance more than inherent optical properties of particles, which were attributed to the proximity of roughness and thickness values to the 100 nm threshold for visible transparency. Samples on PMMA substrates performed modestly better than those on PC and glass in terms of wettability and transmittance. However, all samples exhibited a superhydrophobic CA ( $>150^\circ$ ), low CAH ( $<10^\circ$ ), and high transmittance of visible light ( $>90\%$  in most cases). In addition, all surfaces showed wear resistance for potential commercial use in AFM wear and water jet experiments indicating strong bonding of the silicone resin and sufficient hardness of nanoparticles and resin. They concluded that transparent superhydrophobic surfaces with wear resistance can be fabricated with a broad range of materials to expand potential engineering applications. However, primary particle size, roughness, and coating morphology appear to be at least as important a factor in transparency as inherent optical properties of nanoparticles when coating thickness is on the order of 100 nm.



**Figure 7.** Surface height maps and sample surface profiles (locations indicated by arrows) before and after AFM wear experiment using 15  $\mu\text{m}$  radius borosilicate ball at load of 10  $\mu\text{N}$  for glass samples with silicone resin alone,  $\text{SiO}_2$  nanoparticles, ZnO nanoparticles, and ITO nanoparticles. rms roughness and PV distance values for surface profiles are displayed within surface profile boxes. Results shown are typical for all substrates [33].

Deng et al. [34] presented a simple method to fabricate a superhydrophobic coating based on porous silica capsules (Figure 8). The superhydrophobic coating showed a static contact angle of  $160^\circ$  and sliding angle less than  $5^\circ$ . Moreover, it was thermally stable up to  $350^\circ\text{C}$ . On the other hand, it also acted as anti-fouling layer for solar cells. The superhydrophobic coating did not diminish the efficiency of organic solar cells, also due to its excellent transparency. Further, the coating retained its superhydrophobicity under adhesion tape peeling and sand abrasion tests, which are demonstrated in Figure 8a,b (tape peel) and Figure 8c (sand abrasion).



**Figure 8.** SEM images of superhydrophobic surfaces that were partially exposed to double sided tape (white boxes indicate the exposed areas). (a) If the particles stick to the surface by van der Waals interaction only, they can easily be removed; (b) Particles cannot be removed by double sided tape after binding them chemically to the surface by silica bridges; (c) Sketch of the setup used to determine the stability of the surface against sand impact; (d) Static contact angle and sliding angle measured after annealing the samples for 10 h at different temperatures. The surface remains superhydrophobic until annealing at 350 °C [34].

To improve the mechanical stability of the nanoparticle films, chemical vapor deposition (CVD) of tetraethoxysilane in the presence of ammonia was performed. To quantify the mechanical stability of the surfaces two separate tests were performed. Firstly, double sided adhesive tape is pressed with approximately 10 kPa to the surfaces, both, before and after performing CVD of tetraethoxysilane. If the capsules are attached to the surface by van der Waals interactions only a sharp boundary would be visible, separating areas that are and are not exposed to tape. After peeling the tape off, the area underneath it is almost particle free, substantiating the poor adhesion of the particles to the substrate (white box in Figure 8a). Contrary, if CVD of TES is performed beforehand peeling the tape off does not change the particle coverage (Figure 8b). In a second test, sand grains are impacted on a superhydrophobic surface and the minimal height is determined at which the porous silica particles burst. Bursting led to an increase of the sliding angle and finally to loss of superhydrophobicity. When 100 to 300  $\mu\text{m}$  sized sand grains were impacted on a superhydrophobic surface the shells remained intact for impact heights up to 30 cm. After the sand abrasion the surface remained superhydrophobic, i.e., water droplets placed on the surface can bounce and slide off easily.

Inspired by mussels, Si et al. [35] designed a novel green superhydrophobic nanocoating with good transparency and stability through a facile reaction at room temperature with trimethyl silyl modified process. The nano-coating was coated from ethanol onto various substrates via a simple spray process without requiring toxic substances. The application also rendered the coatings self-healing. The nanocoating demonstrated rapid self-healing superhydrophobicity induced by exposure to organic solvents which can be applied at industrial levels (see Figure 9). At first, silica sol was prepared via a typical tetraethoxysilane (TEOS) hydrolysis reaction in an alkaline environment. After dopamine (DOPA) was added into the silica sol system forming an opaque DOPA–silica gel due to the presence of the –OH groups after ageing. The DOPA–silica gel was reacted with 1,1,1,3,3,3-hexamethyl disilazane (HMDS) to convert the rest of the –OH groups on the surface of the gel to –OSi(CH<sub>3</sub>)<sub>3</sub>. In order to obtain a transparent superhydrophobic nanocoating, the DOPA–silica gel was dried at 60 °C and

ground to get an hydrophobic powder Using environmentally friendly nontoxic ethanol as a solvent, a transparent superhydrophobic DSTM gel nanocoating with varying mass ratios was prepared which was sprayed on various engineering material substrates without any pre-treatment regardless of the composition and morphology. No abrasion related wear tests were conducted on the prepared coatings, the self-healing properties were demonstrated against damage by solvent soaking only.

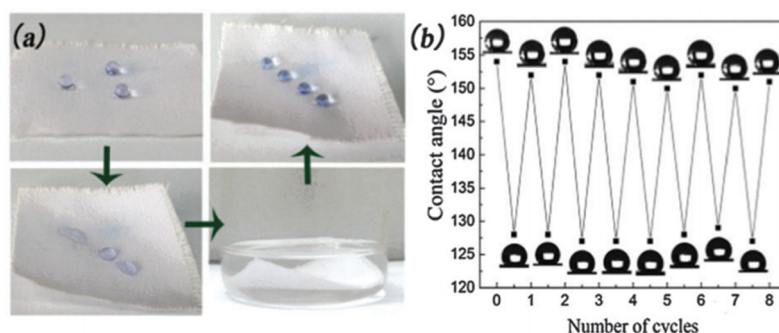


**Figure 9.** (a) Demonstration of self-healing superhydrophobicity of the coated cotton fabric induced by acetone; (b) WCAs on the coated copper wire mesh in the eight cycles of 1 M HCl treatment [35].

Deng et al. [36] designed an easily fabricated, transparent, and oil-rebounding superamphiphobic coating (Figure 10B) using porous deposit of candle soot that was coated with a 25-nanometer-thick silica shell. The black soot-colored coating became transparent after calcination at 600 °C. After silanization, the coating was superamphiphobic and remained so even after its top layer was damaged by sand impingement (Figure 10C). The coating consisted of a fractal-like assembly of nanospheres (Figure 10D). With increasing duration of CVD of TES or annealing above 1100 °C, the necks between particles were filled with silica and more rod-like shapes evolved, which reduced the superamphiphobicity. This was attributed to the notion that convex small-scale roughness can provide a sufficient energy barrier against wetting thus rendering superamphiphobicity possible. The coating was sufficiently oil-repellent to cause the rebound of impacting drops of hexadecane. Even low-surface-tension drops of tetradecane rolled off easily when the surface was tilted by 5°, taking impurities along with them. The surface kept its superamphiphobicity after being annealed at 400 °C.

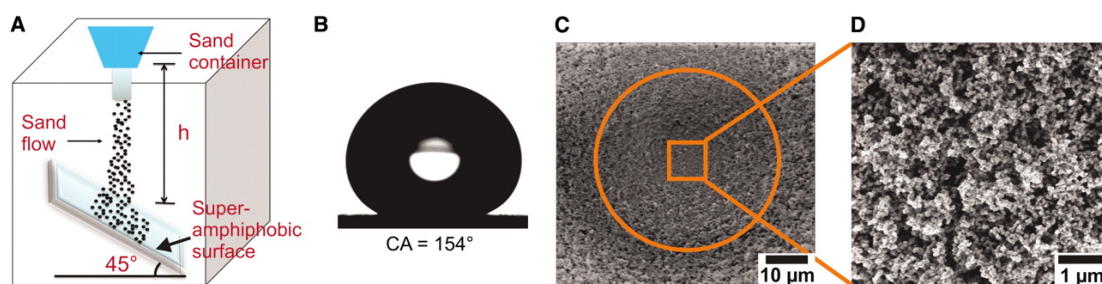


**Figure 10.** Mechanical resistance quantified by sand abrasion. (A) Schematic drawing of a sand abrasion experiment; (B) Hexadecane drop deposited on the coating after 20 g of sand abrasion from 40 cm height. The 100- to 300-µm-sized grains had a velocity of 11 km/hour just before impingement. After impingement, the drops rolled off after the substrate was tilted by 5°; (C) SEM image of a spherical crater (orange circle) after sand abrasion; (D) SEM image of the surface topography inside the cavity [36].

Yokoi et al. [37] produced a superhydrophobic polyester mesh (Figure 11a) possessing both mechanical stability and high transparency in the visible light range by coating 1H,1H,2H,2H-perfluorodecyltrichlorosilane (PFDTs)-treated fibers, after chemical etching, with SiO<sub>2</sub> nanoparticles

functionalized with 1*H*,1*H*,2*H*,2*H*-perfluorooctyltriethoxysilane (PFOTS). It was found that the fabricated mesh maintained its superhydrophobicity and low water sliding angle because of the PFOTS surface treatment, although the SiO<sub>2</sub> nanoparticles modified with PFOTS are removed by the abrasion (Figure 11b). The vacant space between the mesh fibers allowed the penetration of visible light and protected the nanoroughness provided by the SiO<sub>2</sub> nanoparticles. They claimed that it was unnecessary to control the refractive index of the materials for improving transparency and to contain strong chemical or physical bonding between the particles or the particles and the substrate for improving the abrasion resistance. Therefore, compared with the traditional technology, the combination of the see-through mesh and the SiO<sub>2</sub> nanoparticle hierarchical structure appears to be an effective and simple method for improving the abrasion resistance and transparency of these superhydrophobic films (Figure 11c,d).

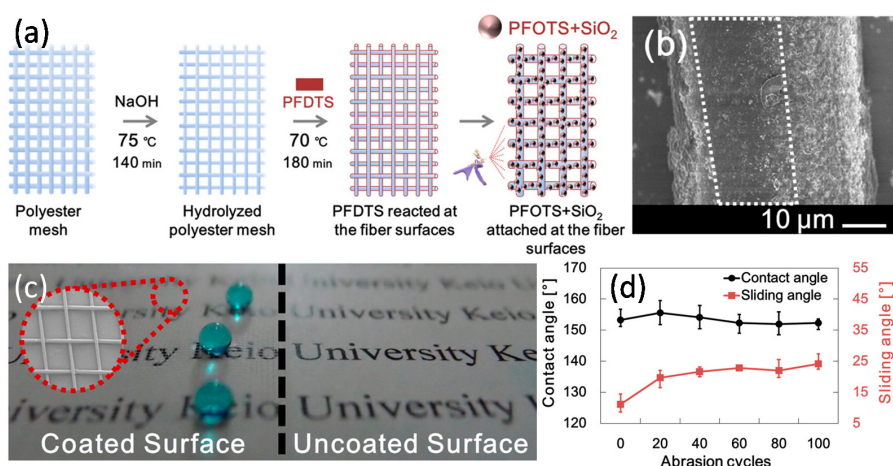


**Figure 11.** (a) Schematic of the fabrication procedure for the superhydrophobic polyester mesh. First, a polyester mesh undergoes an alkaline treatment with NaOH. Second, PFOTS is reacted on the fiber surfaces using the chemical vapor deposition method. Third, the mesh is treated with SiO<sub>2</sub> nanoparticles modified with PFOTS using a spray method; (b) FE-SEM images of the superhydrophobic polyester meshes after 100 cycles of abrasion with a pressure of ~10 kPa. Dashed zone is shows loss of nanoparticle from the fiber surface; (c) Photograph of blue-colored water on the coated polyester mesh surface (left) and a photograph of an uncoated surface on white paper for comparison; (d) Contact angle and sliding angle measurements of the superhydrophobic meshes using aqueous solutions with a pH range of 2–14 [37].

## 5. Transparent Non-Wettable Coatings from Pattern Transfer to Polymers

Gong et al. [38] recently reported a convenient and efficient duplicating method, being capable to form a transparent PDMS surface with superhydrophobicity in mass production. They claimed that the fabrication process had extensive application potentials. They used a femtosecond laser processing to fabricate mirror finished stainless steel templates (Figure 12a) with surface structures combining microgrooves with microholes array. Then liquid PDMS was poured for the duplicating process to introduce a particular structure composed of a microwalls array with a certain distance between each other and a microprotrusion positioned at the center of a plate surrounded by microwalls (Figure 12b,c). The parameters such as the side length of microwalls and the height of a microcone were optimized to achieve required superhydrophobicity at the same time as high-transparency properties (Figure 12d,e). The PDMS surfaces showed superhydrophobicity with a static contact angle of up to  $154.5 \pm 1.7^\circ$  and sliding angle lower to  $6 \pm 0.5^\circ$ , also with a transparency over 91%, a loss less than 1% compared with flat PDMS by the measured light wavelength in the visible light scale (Figure 12f). They tested wear resistance by sandpaper over 100 cycles of abrasion. The superhydrophobic PDMS surfaces were also tested for thermal stability up to 325 °C.

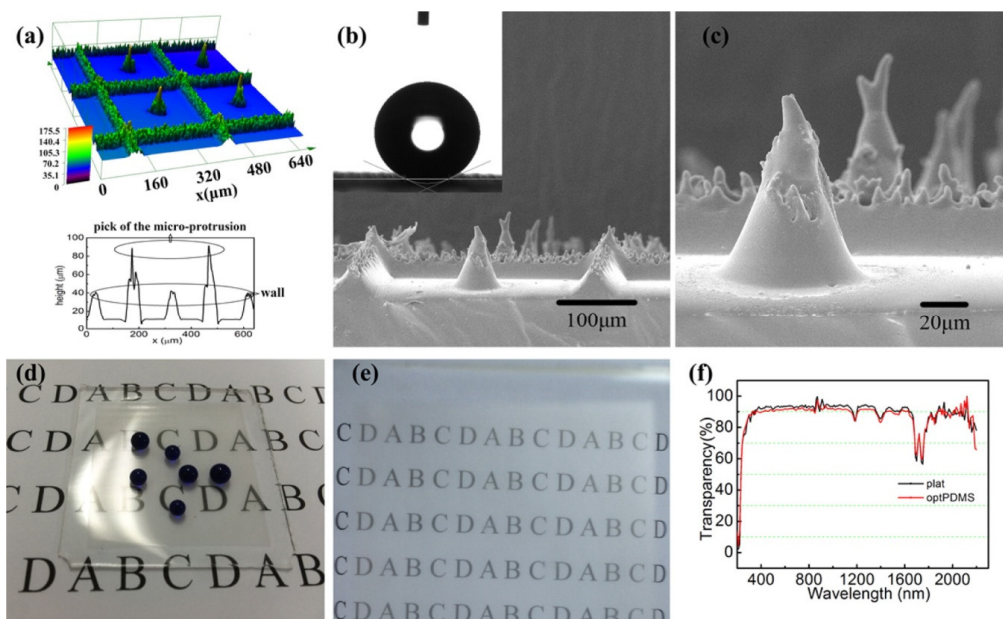


**Figure 12.** Surface microstructure of PDMS as a result of molding into a stainless steel substrate (a) laser microscope and SEM (b) 500× and (c) 2000×. The SCA of this optimal surface is  $154.5^\circ \pm 1.7^\circ$  and SA  $6^\circ \pm 0.5^\circ$ ; (d) Sample of optimally designed PDMS coated on the paper; and (e) it was held up to keep a certain distance (10 cm) from the paper; (f) Transparency of the optimal designed surface is over 91% in the visible light wavelength [38].

Im et al. [39] demonstrated a robust superhydrophobic and superomniphobic surface based on transparent polymer microstructuring (Figure 13). On a large-size template of the transparent polydimethylsiloxane (PDMS) elastomer surface, perfectly ordered microstructures with an inverse-trapezoidal cross section were fabricated with two consecutive PDMS replication processes and a three-dimensional diffuser lithography technique. Figure 13 demonstrates a schematic representation of these surface patterns. The hydrophobicity and transparency were improved by additional coating of a fluoropolymer layer. The robustness of superhydrophobicity was confirmed by the water droplet impinging test. Additionally, the fabricated superhydrophobic surface was also superomniphobic, which shows a high contact angle with a low surface tension ( $\gamma_{la}$ ) liquid, such as methanol ( $\gamma_{la} = 22.7 \text{ mN}\cdot\text{m}^{-1}$ ).

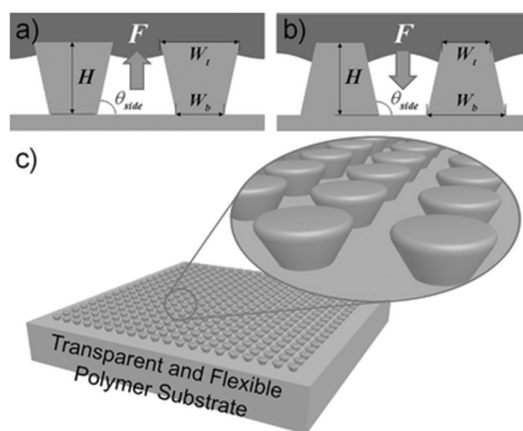


**Figure 13.** Water meniscus and the net force on: (a) overhang structures ( $W_t > W_b$ ); (b) structures like truncated pyramids with inclined sidewalls ( $W_t < W_b$ ); (c) Schematic illustration of the PDMS trapezoids surface [39].

The authors did not present any durability or mechanical wear or abrasion results but the intrinsic properties of PDMS rubber should dictate a certain degree of resilience against rubbing induced wear or abrasion.

Kim et al. [40] demonstrated highly transparent super-hydrophobic surface fabrication approach using nanoimprint lithography with a flexible mold (see Figure 14). They also applied a PDMS-based coating to achieve both a highly transparent super-hydrophobic surface and an anti-adhesion layer coating for high-resolution nanoimprint lithography by intrinsic low surface energy and easy release of PDMS. The PDMS-coated flexible mold was used repeatedly, more than 10 times, without losing the anti-adhesion property of PDMS and endured severe chemical cleaning processes, such as sonication, which were performed periodically to wash the mold after several consecutive imprinting.

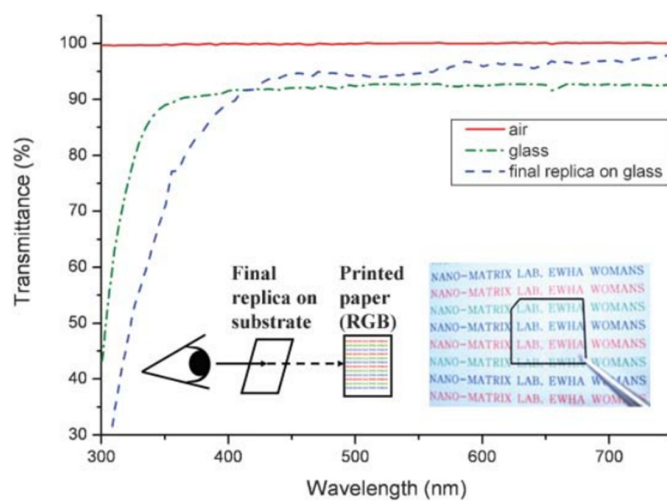


**Figure 14.** The transmittance of the highly transparent super-hydrophobic surface and a photograph of letters underneath the transparent superhydrophobic film [40].

They claimed that this process could be suitable for various applications that require both super-hydrophobic and anti-reflective surface coatings. Further, they claimed that the process could be easily extended to a large area patterning; therefore, this method could be suitable for mass production of nanopatterned polymeric optical substrates, and could be applicable towards solar cell surface contamination and plastic optics which require dust-free and self-cleaning surfaces with high transmission. They did not report any performance data on abrasion induced wear resistance on these materials.

Dufour et al. [41] conducted a systematic study on mushroom shaped (with sharper microscale reentrant shapes compared to Figure 13) PDMS molds functionalized with 1H,1H,2H,2H-perfluorodecyltrichlorosilane in vapor phase. They used low surface tension liquids (down to 28 mN/m) in their wetting analysis. In summary, on these mushroom-like PDMS surfaces, they concluded that since the contact line was always pinned around the cap contour, variation of apparent static contact angle with the liquid surface tension was negligible. Consequently, contact angle hysteresis was relatively large even for water. These microstructures were able to sustain a composite interface (an intermediate wetting state) with liquids having surface tension down to 27.9 mN/m, but as soon as the state became unstable, the drop completely spread into the lattice. The transition from Cassie-Baxter to Wenzel state was discontinuous, and there was no intermediate metastable configuration (partial impalement). Thus, the superomniphobic property of PDMS microstructures was attributed to their ability to prevent local Cassie Baxter-Wenzel transition since lateral spreading occurred immediately after the composite interface disappeared.

## 6. Transparent Non-Wettable Coatings from Ceramic-Based Nanostructures

The design and development of robust self-cleaning coatings for use in solar panels or solar cells is especially important given that nearly half of the overall power conversion efficiency of solar panels can be lost due to dust or dirt accumulation every year. In fact, some solar panels are known to be protected well with certain transparent anti-graffiti coatings. In addition to water- and dust-repellent property requirements, superhydrophobic coatings for photovoltaics must be highly transparent to both visible and near-IR light as well as being UV-resistant and durable. One promising approach [42] fabricated highly transparent porous silica coatings on glass substrates through layer-by-layer (LbL) assembly of raspberry-like polystyrene@silica (PS@SiO<sub>2</sub>) microparticles followed by calcination at high temperature. Initially the coatings were superhydrophilic but became superhydrophobic after chemical vapor deposition of 1H,1H,2H,2H-perfluorodecyltriethoxysilane. Superhydrophobic porous silica coating had a water contact angle greater than 160° with a sliding angle of 7° and a transmittance of 85%. The authors claimed that transparency can be increased by lowering the LbL cycles but did not demonstrate superhydrophobic coatings with higher transparency.

Gao et al. [43] fabricated highly transparent and UV-resistant superhydrophobic arrays of SiO<sub>2</sub>-coated ZnO nanorods that were prepared in a sequence of low-temperature (<150 °C) steps on both glass and thin sheets of polyester, PET (2 × 2 in.<sup>2</sup>), and the superhydrophobic nanocomposite is shown to have minimal impact on solar cell device performance under AM1.5G illumination (See Figure 15a). They argued that such flexible plastics can serve as front cell and backing materials in the manufacture of flexible displays and solar cells. To demonstrate the minimal impact of the presence of the superhydrophobic nanorod arrays on solar cell performance, they prepared bulk-heterojunction (BHJ) devices with the polymer donor PBDTTPD and the fullerene acceptor PC71BM. The configuration of the OPV device including the SiO<sub>2</sub>/ZnO nanocomposite is shown in Figure 15a; Figure 15b shows perfectly spherical droplets positioned on the front of the superhydrophobic device (static angle, 157°; sliding angle, 13°). The superhydrophobic cell (red curve, circles) and bare reference cell (blue curve, squares) under AM1.5G solar illumination (100 mW·cm<sup>-2</sup>) (Figure 15c) exhibit equivalent current-voltage characteristics with comparable power conversion efficiencies (PCEs) of 6.9% and 6.8%, respectively, values comparable within the limits of experimental accuracy. In parallel, their external quantum efficiency (EQE) spectra (Figure 15d) show comparably broad and efficient EQE responses, with values >60% in the 370–630 nm range, and peaking at ca. 70% at 550 nm, which confirms the minimal impact of the presence of the superhydrophobic nanorod arrays on solar cell performance. They did not present any results on the durability of these coatings against abrasion.

Although no abrasion induced wear resistance tests were conducted, bending resistance of the transparent (Figure 14c,d) non-wettable coatings were demonstrated by the authors as seen in Figure 14c. They claimed that such robustness is important for flexible solar energy converters.

Yadav et al. [44] reported the emergence of superhydrophobic wetting behavior and enhanced UV stability of indium oxide (IO) nanorods due to their vertical alignment (Figure 16). Both randomly distributed and vertically aligned IO nanorods were synthesized (Figure 16a,b) via chemical vapor deposition (CVD) method. Their results showed that the static water contact angle (WCA) demonstrated a significant dependence on the alignment of the nanorods. The randomly distributed IO nanorods had 133.7° ± 6.8° wetting whereas for vertically aligned IO nanorods WCA was found to be 159.3° ± 4.8°. Continuous UV light illumination for 30 min exhibited the change in contact angle (ΔWCA) of about 41° for vertically aligned IO nanorods whereas randomly distributed IO nanorods become hydrophilic with a dramatic change in WCA value of 108°. The superhydrophobicity of vertically aligned IO nanorods and their enhanced UV stability were discussed by comparing the effective solid fraction at solid-liquid interface and the reactivity of surface crystallographic planes. They argued that the superhydrophobic surface of aligned vertically standing IO nanorods along with its resistance against photoinduced wetting transition can make them suitable for electronic devices with reduced surface discharge even at relatively high humidity levels. They did not test and measure any results related to mechanical durability of their coatings.

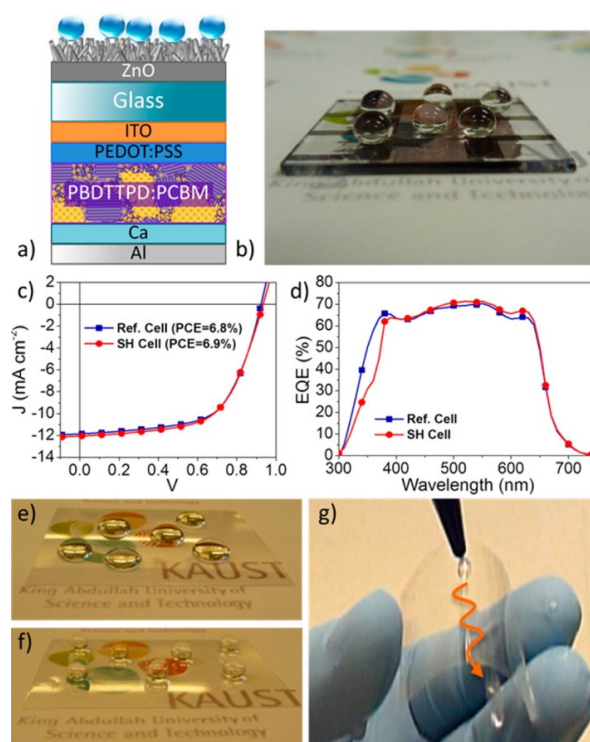


**Figure 15.** (a) Schematic of a BHJ polymer solar cell including the  $\text{SiO}_2/\text{ZnO}$  nanocomposite; (b) Water droplets positioned on the front of the superhydrophobic device remain perfectly spherical; (c)  $J$ - $V$  characteristic of a superhydrophobic (SH) cell (red circle) superimposed on that of a bare reference (Ref.) cell (blue square); AM1.5G solar illumination ( $100 \text{ mW}\cdot\text{cm}^{-2}$ ); (d) EQE spectra of the SH cell (red circle) and the Ref. cell (blue square); (e) Water droplets positioned on a bare transparent sheet of PET ( $2 \times 2 \text{ in.}^2$ ); (f) Droplets positioned on superhydrophobic PET (static angle:  $160^\circ$ ); (g) PET retains its superhydrophobicity upon repeated bending ( $\times 350$ ) [43].

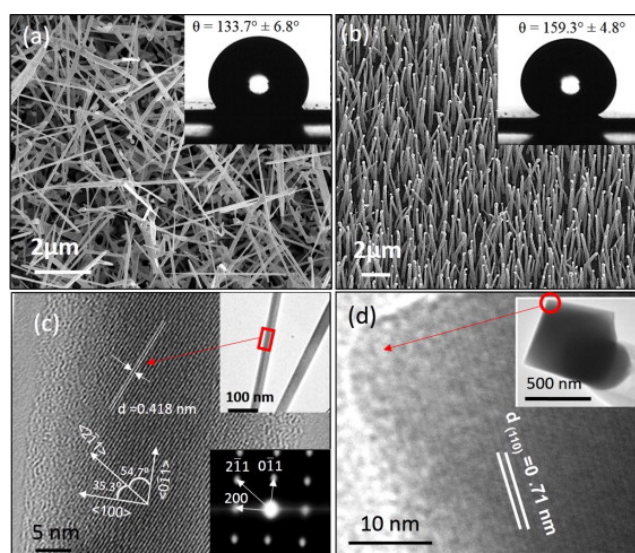


**Figure 16.** FESEM images of (a) randomly distributed and (b) vertically aligned IO nanorods. The insets show the contact angle images of the respective samples. HRTEM images of (c) randomly distributed and (d) vertically standing IO nanorods. The insets show the TEM and SAED pattern of respective nanorods [44].

Aytug et al. [45] reported the formation of low-refractive index antireflective glass films that embody omni-directional optical properties over a wide range of wavelengths, while also possessing specific wetting capabilities. The coatings were made up of an interconnected network of nanoscale pores surrounded by a nanostructured silica framework. These structures came from a method that exploited metastable spinodal phase separation in glass-based materials. Their approach not only enabled design of surface microstructures with graded-index antireflection characteristics, where the surface reflection was suppressed through optical impedance matching between interfaces, but also enabled self-cleaning ability through modification of the surface chemistry. Based on near complete elimination of Fresnel reflections (yielding >95% transmission through a single-side coated glass) and corresponding increase in broadband transmission, the fabricated nanostructured surfaces were found to promote a general and an invaluable ~3%–7% relative increase in current output of multiple direct/indirect bandgap photovoltaic cells. Moreover, these antireflective surfaces also demonstrated superior resistance against mechanical wear and abrasion. Their antireflective coatings were essentially monolithic, enabling simultaneous realization of graded index anti-reflectivity, self-cleaning capability, and mechanical stability within the same surface.

Figure 17a shows typical indenter generated scanning probe microscopy images of scratch tracks for a sputter deposited film, a fully processed film (i.e., heat treated and etched), and the underlying borosilicate substrate. The scratches, produced after the application of load ramped up to the equipment peak of 10,000  $\mu\text{N}$ , showed no evidence of cracking, brittle fragmentation or tendency toward delamination. Moreover, for loads at one-half and at full equipment maximum the average penetration depth (calculated from the lateral and vertical displacements) of the indenter is nearly the same for both the reference substrate and the coated sample. This result suggests that the scratch resistance behavior of the as-deposited films is similar to that of the underlying substrate material. Accordingly, the coefficient of friction profiles for a representative template revealed similar behavior, as displayed in Figure 17b. Such transparent (Figure 17c), robust and low friction coefficient coatings do have potential as preventive treatments for anti-graffiti applications particularly for public transportation vehicle windows.

Metal oxides, in general, are known to exhibit significant wettability towards water molecules because of the high possibility of synergetic hydrogen-bonding interactions at the solid-water interface. Very recently, Sankar et al. [46] showed that nano sized phosphates of rare earth materials (Rare Earth Phosphates, REPs),  $\text{LaPO}_4$  in particular, exhibited without any chemical modification, unique combination of intrinsic properties including notable hydrophobicity that could be retained even after exposure to extreme temperatures and harsh hydrothermal conditions (Figure 18a). Nanostructured film surface is depicted in Figure 18b. Transparent nanocoatings of  $\text{LaPO}_4$  as well as mixture of other REPs on glass surfaces were shown to display hydrophobicity with water contact angle (WCA) value of  $120^\circ$  (Figure 18c) while sintered and polished monoliths manifested WCA greater than  $105^\circ$ . Significantly, these materials in the form of coatings and monoliths also exhibited complete non-wettability and inertness towards molten metals like Ag, Zn, and Al well above their melting points. They proposed that these properties, coupled with their excellent chemical and thermal stability, ease of processing, machinability and their versatile photo-physical and emission properties, render  $\text{LaPO}_4$  and other REP ceramics utility in diverse applications.

The crystalline structure of the films ( $\text{LaPO}_4$ ,  $\text{GaPO}_4$ ,  $\text{NdPO}_4$ ) is depicted in Figure 18d. They did not conduct any kind of mechanical wear abrasion tests on these interestingly hydrophobic inorganic coatings. However, due to their ceramic nature these films are expected to have satisfactory resistance to abrasion induced wear or scratches. Nonetheless, such tribological experiments should also be reported.

Fukada et al. [47] developed semi-transparent superomniphobic surfaces and applied as coating to integrate antifouling properties in solar cell devices. The coatings featured mesh and stripe structures (see Figure 19a,b). The stripe structure was more suitable for generating transparent and highly oleophobic coatings (Figure 19c), thereby displaying excellent antifouling properties. The stripe-based

coating also displayed good thermally stability. Total transmittance was a key factor influencing the conversion efficiency. By applying an antifouling treatment, reduction in the performance of the solar cell devices was inhibited. For instance, the stripe-coated solar cells maintained a high conversion efficiency of 92% of the non-coated solar cell even in the presence of oil contaminant. In contrast, in the absence of the stripe substrate, conversion efficiency decreased to 64%.

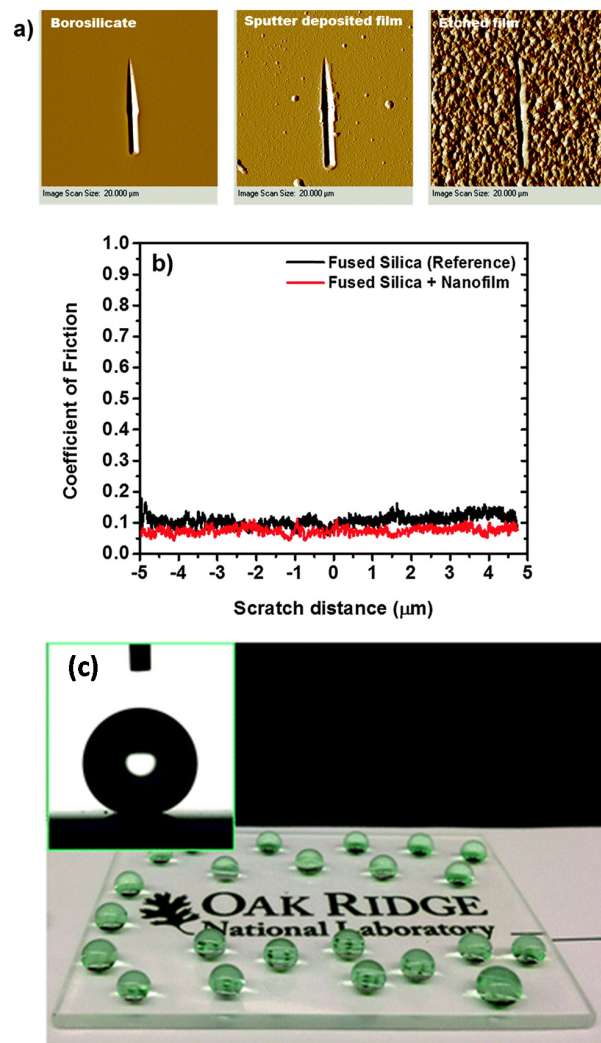


**Figure 17.** (a) Topographical images of the scratches made on an as-deposited and a nanotextured glass thin film. Image for the underlying uncoated borosilicate substrate is also included for comparison. No debris is observed on any sample, aside from several small and large sized surface-bound particles on the sputtered film. Note that the as-sputtered borosilicate films are generally somewhat rougher than the underlying substrates; (b) Comparison of the coefficient of friction profiles as a function of scratch distance for fused silica substrates with and without a dense borosilicate film; (c) Photograph of blue dyed water droplets on a borosilicate substrate coated with nanoporous antireflective glass film. The film surface is modified by a covalently bonded organosilane chemistry. Inset shows the profile of a 5  $\mu$ L water droplet resting on a similarly processed film, displaying a static contact angle of 165° [45].

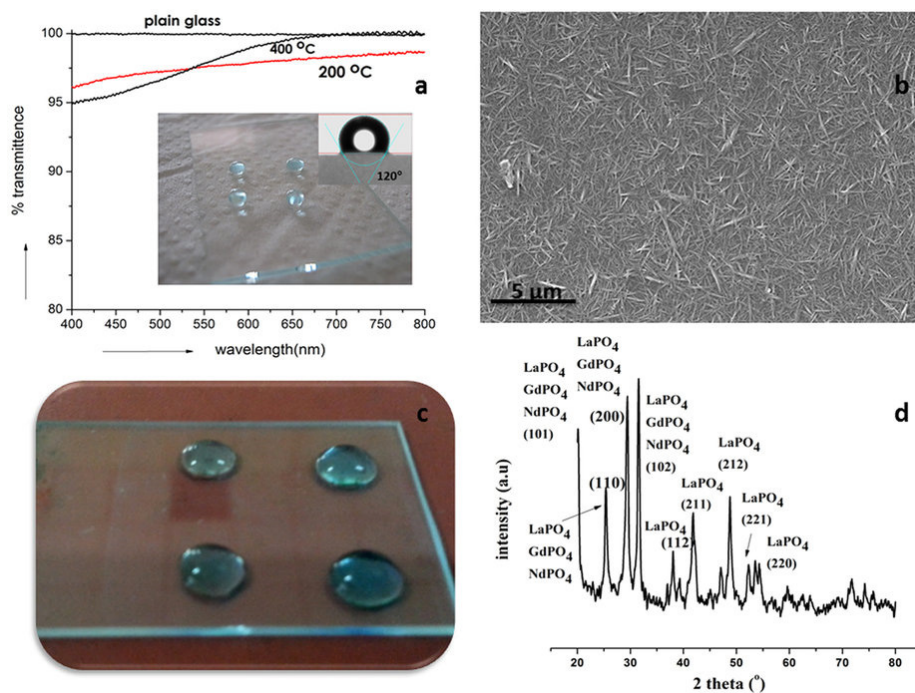


**Figure 18.** Hydrophobicity achieved for LaPO<sub>4</sub> coated thin film. (a) Water droplets sitting over LaPO<sub>4</sub> coated glass plate and the high optical transparency recorded for the films; (b) SEM image showing spike-like arrangement of LaPO<sub>4</sub> nanorods over the glass surface; (c) Mixed REP sol coated glass slide showing hydrophobic character; (d) Diffraction pattern obtained for mixed rare earth phosphates [46].

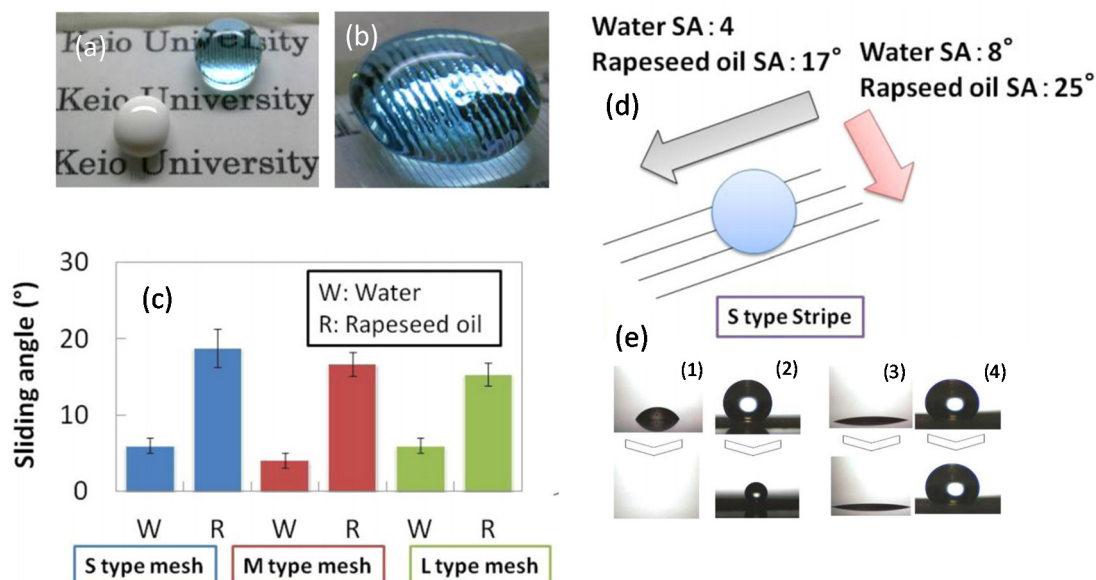


**Figure 19.** (a) Methylene blue-stained water and white ink stained rapeseed oil on a stripe substrate and (b) enlarged stripe structure in the presence of water; (c) Sliding angle measurements; (d) The droplet of water or rapeseed oil was placed on the mesh/stripe substrate. The substrate was then tilted slowly and the angle was measured when the liquid moved. (e) Thermal stability of mesh and stripe substrates, examined at 80 °C for 10 min. (1) Water (10 μL) on glass, the CA was 44°; (2) Water (10 μL) on L-type mesh, CA was changed from 151.6° to 146.0°; (3) Rapeseed oil (10 μL) on glass, CA was changed from <5.0° to <5.0°; (4) Rapeseed oil (10 μL) on L-type mesh, CA was changed from 141.9° to 141.0° [47].

## 7. Recommendations for Future Directions

Over the last decade and particularly in the last five years, many efficient methods of producing transparent non-wettable surfaces have been demonstrated. Most of the methods reviewed above are still not suitable for sustained mechanical durability against abrasion induced wear. As a future direction, the most important aspect would be to focus on substrate adhesion improvements of nanoparticle films. These could be done by applying transparent primers or adhesive layers or by welding the nanoparticles into transparent polymeric substrates by thermal annealing methods. The second important point would be to maintain “wear independent texture similarity” discussed earlier. In other words, the surface of the coatings or the films may wear away but the newly exposed layers can still have hierarchical texture with hydrophobic chemistry. In the case of dynamic oleophobicity (non-stick oil droplets), more environmentally friendly chemicals should be used rather than C-8 based fluorinated oils or silanes.

Furthermore, researchers should use established mechanical durability testing methods such as ASTM standards of paint industry instead of homemade tests such as running sandpaper over the non-wettable coating or film. Type of the abradant used as well as the downward pressure should always be indicated otherwise cross-comparisons may not be possible. A standard wear abrasion test should be the primary indicator to label non-wettable coatings as *mechanically durable* but secondary tests such as substrate adhesion, scratch resistance; powder and/or rain/spray erosion tests should also be conducted and reported. All in all, studies to date still lack these features and as such it is still not possible to attract industrial attention to produce robust commercial transparent non-wettable coatings for outdoor installations.

## 8. Conclusions and Outlook

In this review, we attempted to present the state-of-the-art in fabricating and testing transparent hydrophobic, superhydrophobic and oleophobic coatings against mechanical durability in terms of wear and abrasion resistance. Review of recent literature indicates that most of the published works have not presented any performance results related to resilience against abrasion induced wear [48]. Reports on fluorinated oil infused transparent nanotextured surfaces also exist [49], which claim excellent outdoor performance and substrate independent universal fabrication, but with no abrasion induced wear resistance characterization. However, dynamically oleophobic surfaces deserve mention here [50]. Dynamically oleophobic surfaces (mostly transparent) do not present hierarchical surface textures, in general, but low surface tension hydrocarbon liquid droplets bead up instead of spreading and can still slide away and clear such surfaces. This approach could be good against oil-based paint stain resistance on outdoor installations. Moreover, some of these environmentally friendly coatings have been designed to display excellent thermal stability, dynamic/thermoresponsive oleophobicity, and hydrolytic stability [51]. Perhaps, solid-air interfaces with dynamic oleophobicity that are generally grown from precursors can be similarly grown on wear abrasion resistant transparent coating textures so that oil-based stains can also be prevented on wear resistant transparent coatings. We identified three major fabrication methods namely, nanoparticle assembly and films, transparent elastomer surface micro/nano structuring by molding and formation of nanostructured ceramic surfaces functionalized with hydrophobic macromolecules, suitable for solar energy conversion devices. The relevance of this review to anti-graffiti applications stems from the fact that transparency maintains see-thru properties after the coatings are applied and in certain cases the oleophobicity results in not only water repellence but also grease/dirt repellence.

As summarized above, combining transparency with mechanical abrasion resistance (important for anti-graffiti applications) is very challenging and is not described frequently. However, latest reports indicate considerable progress towards achieving both in one layer coating. It is also important to note that most of these fabrication methods should eventually translate into and applied over large areas commonly encountered for graffiti prevention; in other words, public transport vehicle windows, walls, or building windows, to name a few. Although such an immediate transformation is premature

currently, future approaches should also address this need so that more industrial interest can be attracted towards joint development efforts.

**Conflicts of Interest:** The author declares no conflict of interest.

## References

1. Tserepi, A.D.; Vlachopoulou, M.E.; Gogolides, E. Nanotexturing of poly (dimethylsiloxane) in plasmas for creating robust super-hydrophobic surfaces. *Nanotechnology* **2006**, *17*, 3977–3984. [[CrossRef](#)]
2. Wang, D.; Zhang, Z.; Li, Y.; Xu, C. Highly transparent and durable superhydrophobic hybrid nanoporous coatings fabricated from polysiloxane. *Appl. Mater. Interfaces* **2014**, *6*, 10014–10021. [[CrossRef](#)] [[PubMed](#)]
3. Tuvshindorj, U.; Yildirim, A.; Ozturk, F.E.; Bayindir, M. Robust cassie state of wetting in transparent superhydrophobic coatings. *Appl. Mater. Interfaces* **2014**, *6*, 9680–9688. [[CrossRef](#)] [[PubMed](#)]
4. Yabu, H.; Shimomura, M. Single-step fabrication of transparent superhydrophobic porous polymer films. *Chem. Mater.* **2005**, *17*, 5231–5234. [[CrossRef](#)]
5. Liu, Y.; Das, A.; Xu, S.; Lin, Z.; Xu, C.; Wang, Z.L.; Rohatgi, A.; Wong, C.P. Hybridizing ZnO nanowires with micropylar silicon wafers as superhydrophobic high-efficiency solar cells. *Adv. Energy Mater.* **2012**, *2*, 47–51. [[CrossRef](#)]
6. Giolando, D.M. Transparent self-cleaning coating applicable to solar energy consisting of nano-crystals of titanium dioxide in fluorine doped tin dioxide. *Sol. Energy* **2016**, *124*, 76–81. [[CrossRef](#)]
7. Bayer, I.S.; Megaridis, C.M.; Zhang, J.; Gamota, D.; Biswas, A. Analysis and surface energy estimation of various model polymeric surfaces using contact angle hysteresis. *J. Adhes. Sci. Technol.* **2007**, *21*, 1439–1467. [[CrossRef](#)]
8. Milionis, A.; Bayer, I.S.; Loth, E. Recent advances in oil-repellent surfaces. *Int. Mater. Rev.* **2016**, *61*, 101–126. [[CrossRef](#)]
9. Steele, A.; Davis, A.; Kim, J.; Loth, E.; Bayer, I.S. Wear independent similarity. *Appl. Mater. Interfaces* **2015**, *7*, 12695–12701. [[CrossRef](#)] [[PubMed](#)]
10. Milionis, A.; Loth, E.; Bayer, I.S. Recent advances in the mechanical durability of superhydrophobic materials. *Adv. Colloid Interface Sci.* **2016**, *229*, 57–79. [[CrossRef](#)] [[PubMed](#)]
11. Milionis, A.; Languasco, J.; Loth, E.; Bayer, I.S. Analysis of wear abrasion resistance of superhydrophobic acrylonitrile butadiene styrene rubber (ABS) nanocomposites. *Chem. Eng. J.* **2015**, *281*, 730–738. [[CrossRef](#)]
12. Milionis, A.; Dang, K.; Prato, M.; Loth, E.; Bayer, I.S. Liquid repellent nanocomposites obtained from one-step water-based spray. *J. Mater. Chem. A* **2015**, *3*, 12880–12889. [[CrossRef](#)]
13. Herminghaus, S. Roughness-induced non-wetting. *Europhys. Lett.* **2000**, *52*, 165–170. [[CrossRef](#)]
14. Marmur, A. The lotus effect: Superhydrophobicity and metastability. *Langmuir* **2004**, *20*, 3517–3519. [[CrossRef](#)] [[PubMed](#)]
15. Bico, J.; Thiele, U.; Quéré, D. Wetting of textured surfaces. *Colloids Surf. A* **2002**, *206*, 41–46. [[CrossRef](#)]
16. Xiu, Y.; Liu, Y.; Hess, D.W.; Wong, C.P. Mechanically robust superhydrophobicity on hierarchically structured Si surfaces. *Nanotechnology* **2010**, *21*, 155705. [[CrossRef](#)] [[PubMed](#)]
17. Sidorenko, A.; Ahn, H.S.; Kim, D.I.; Yang, H.; Tsukruk, V.V. Wear stability of polymer nanocomposite coatings with trilayer architecture. *Wear* **2002**, *252*, 946–955. [[CrossRef](#)]
18. Schaeffer, D.A.; Polizos, G.; Smith, D.B.; Lee, D.F.; Hunter, S.R.; Datskos, P.G. Optically transparent and environmentally durable superhydrophobic coating based on functionalized SiO<sub>2</sub> nanoparticles. *Nanotechnology* **2015**, *26*, 055602. [[CrossRef](#)] [[PubMed](#)]
19. Mates, J.E.; Bayer, I.S.; Palumbo, J.M.; Carroll, P.J.; Megaridis, C.M. Extremely stretchable and conductive water-repellent coatings for low-cost ultra-flexible electronics. *Nat. Commun.* **2015**, *6*, 8874. [[CrossRef](#)] [[PubMed](#)]
20. Bhushan, B.; Nosonovsky, M. The rose petal effect and the modes of superhydrophobicity. *Philos. Trans. R. Soc. Lond. A* **2010**, *368*, 4713–4728. [[CrossRef](#)] [[PubMed](#)]
21. Bormashenko, E.; Starov, V. Impact of surface forces on wetting of hierarchical surfaces and contact angle hysteresis. *Colloid Polym. Sci.* **2013**, *291*, 343–346. [[CrossRef](#)]

22. Liu, S.; Liu, X.; Latthe, S.S.; Gao, L.; An, S.; Yoon, S.S.; Liu, B.; Xing, R. Self-cleaning transparent superhydrophobic coatings through simple sol-gel processing of fluoroalkylsilane. *Appl. Surf. Sci.* **2015**, *351*, 897–903. [[CrossRef](#)]
23. Rahmawan, Y.; Xu, L.; Yang, S. Self-assembly of nanostructures towards transparent, superhydrophobic surfaces. *J. Mater. Chem. A* **2013**, *1*, 2955–2969. [[CrossRef](#)]
24. Si, Y.; Guo, Z. Superhydrophobic nanocoatings: From materials to fabrications and to applications. *Nanoscale* **2015**, *7*, 5922–5946. [[CrossRef](#)] [[PubMed](#)]
25. Irzh, A.; Ghindes, L.; Gedanken, A. Rapid deposition of transparent super-hydrophobic layers on various surfaces using microwave plasma. *Appl. Mater. Interfaces* **2011**, *3*, 4566–4572. [[CrossRef](#)] [[PubMed](#)]
26. Bravo, J.; Zhai, L.; Wu, Z.; Cohen, R.E.; Rubner, M.F. Transparent superhydrophobic films based on silica nanoparticles. *Langmuir* **2007**, *23*, 7293–7298. [[CrossRef](#)] [[PubMed](#)]
27. Wong, J.X.; Wong, H.; Yu, H.-Z. Preparation of transparent superhydrophobic glass slides: Demonstration of surface chemistry characteristics. *J. Chem. Educ.* **2013**, *90*, 1203–1206. [[CrossRef](#)]
28. Erbil, H.Y.; Cansoy, C.E. Range of applicability of the Wenzel and Cassie-Baxter equations for superhydrophobic surfaces. *Langmuir* **2009**, *25*, 14135–14145. [[CrossRef](#)] [[PubMed](#)]
29. Xu, L.; Karunakaran, R.G.; Guo, J.; Yang, S. Transparent, superhydrophobic surfaces from one-step spin coating of hydrophobic nanoparticles. *Appl. Mater. Interfaces* **2012**, *4*, 1118–1125. [[CrossRef](#)] [[PubMed](#)]
30. Xu, L.; He, J. Fabrication of highly transparent superhydrophobic coatings from hollow silica nanoparticles. *Langmuir* **2012**, *28*, 7512–7518. [[CrossRef](#)] [[PubMed](#)]
31. Zhu, X.; Zhang, Z.; Ren, G.; Men, X.; Ge, B.; Zhou, X. Designing transparent superamphiphobic coatings directed by carbon nanotubes. *J. Colloid Interface Sci.* **2014**, *421*, 141–145. [[CrossRef](#)] [[PubMed](#)]
32. Ling, X.Y.; Phang, I.Y.; Vancso, G.J.; Huskens, J.; Reinhoudt, D.N. Stable and transparent superhydrophobic nanoparticle films. *Langmuir* **2009**, *25*, 3260–3263. [[CrossRef](#)] [[PubMed](#)]
33. Ebert, D.; Bhushan, B. Transparent, superhydrophobic, and wear-resistant coatings on glass and polymer substrates using SiO<sub>2</sub>, ZnO, and ITO nanoparticles. *Langmuir* **2012**, *28*, 11391–11399. [[CrossRef](#)] [[PubMed](#)]
34. Deng, X.; Mammen, L.; Zhao, Y.; Lellig, P.; Müllen, K.; Li, C.; Butt, H.-J.; Vollmer, D. Transparent, thermally stable and mechanically robust superhydrophobic surfaces made from porous silica capsules. *Adv. Mater.* **2011**, *23*, 2962–2965. [[CrossRef](#)] [[PubMed](#)]
35. Si, Y.; Zhu, H.; Chen, L.; Jiang, T.; Guo, Z. A multifunctional transparent superhydrophobic gel nanocoating with self-healing properties. *Chem. Commun.* **2015**, *51*, 16794–16797. [[CrossRef](#)] [[PubMed](#)]
36. Deng, X.; Mammen, L.; Butt, H.J.; Vollmer, D. Candle soot as a template for a transparent robust superamphiphobic coating. *Science* **2012**, *335*, 67–70. [[CrossRef](#)] [[PubMed](#)]
37. Yokoi, N.; Manabe, K.; Tenjimbayashi, M.; Shiratori, S. Optically transparent superhydrophobic surfaces with enhanced mechanical abrasion resistance enabled by mesh structure. *Appl. Mater. Interfaces* **2015**, *7*, 4809–4816. [[CrossRef](#)] [[PubMed](#)]
38. Gong, D.; Long, J.; Jiang, D.; Fan, P.; Zhang, H.; Li, L.; Zhong, M. Robust and stable transparent superhydrophobic polydimethylsiloxane films by duplicating via a femtosecond laser-ablated template. *Appl. Mater. Interfaces* **2016**, *8*, 17511–17518. [[CrossRef](#)] [[PubMed](#)]
39. Im, M.; Im, H.; Lee, J.H.; Yoon, J.B.; Choi, Y.K. A robust superhydrophobic and superoleophobic surface with inverse-trapezoidal microstructures on a large transparent flexible substrate. *Soft Matter* **2010**, *6*, 1401–1404. [[CrossRef](#)]
40. Kim, M.; Kim, K.; Lee, N.Y.; Shin, K.; Kim, Y.S. A simple fabrication route to a highly transparent super-hydrophobic surface with a poly (dimethylsiloxane) coated flexible mold. *Chem. Commun.* **2007**, *22*, 2237–2239. [[CrossRef](#)] [[PubMed](#)]
41. Dufour, R.; Perry, G.; Harnois, M.; Coffinier, Y.; Thomy, V.; Senez, V.; Boukherroub, R. From micro to nano reentrant structures: Hysteresis on superomphobic surfaces. *Colloid Polym. Sci.* **2013**, *291*, 409–415. [[CrossRef](#)]
42. Shang, Q.; Zhou, Y. Fabrication of transparent superhydrophobic porous silica coating for self-cleaning and anti-fogging. *Ceram. Int.* **2016**, *42*, 8706–8712. [[CrossRef](#)]
43. Gao, Y.; Gereige, I.; El Labban, A.; Cha, D.; Isimjan, T.T.; Beaujuge, P.M. Highly transparent and UV-resistant superhydrophobic SiO<sub>2</sub>-coated ZnO nanorod arrays. *Appl. Mater. Interfaces* **2014**, *6*, 2219–2223. [[CrossRef](#)] [[PubMed](#)]

44. Yadav, K.; Mehta, B.R.; Singh, J.P. Superhydrophobicity and enhanced UV stability in vertically standing indium oxide nanorods. *Appl. Surf. Sci.* **2015**, *346*, 361–365. [[CrossRef](#)]
45. Aytug, T.; Lupini, A.R.; Jellison, G.E.; Joshi, P.C.; Ivanov, I.H.; Liu, T.; Wang, P.; Menon, R.; Trejo, R.M.; Lara-Curzio, E.; et al. Monolithic graded-refractive-index glass-based antireflective coatings: Broadband/omnidirectional light harvesting and self-cleaning characteristics. *J. Mater. Chem. C* **2015**, *3*, 5440–5449. [[CrossRef](#)]
46. Sankar, S.; Nair, B.N.; Suzuki, T.; Anilkumar, G.M.; Padmanabhan, M.; Hareesh, U.N.S.; Warriar, K.G. Hydrophobic and metallophobic surfaces: Highly stable non-wetting inorganic surfaces based on lanthanum phosphate nanorods. *Sci. Rep.* **2016**, *6*. [[CrossRef](#)] [[PubMed](#)]
47. Fukada, K.; Nishizawa, S.; Shiratori, S. Antifouling property of highly oleophobic substrates for solar cell surfaces. *J. Appl. Phys.* **2014**, *115*. [[CrossRef](#)]
48. Cao, L.; Gao, D. Transparent superhydrophobic and highly oleophobic coatings. *Faraday Discuss.* **2010**, *146*, 57–65. [[CrossRef](#)] [[PubMed](#)]
49. Ma, W.; Higaki, Y.; Otsuka, H.; Takahara, A. Perfluoropolyether-infused nano-texture: A versatile approach to omniphobic coatings with low hysteresis and high transparency. *Chem. Commun.* **2013**, *49*, 597–599. [[CrossRef](#)] [[PubMed](#)]
50. Park, J.; Urata, C.; Masheder, B.; Cheng, D.F.; Hozumi, A. Long perfluoroalkyl chains are not required for dynamically oleophobic surfaces. *Green Chem.* **2013**, *15*, 100–104. [[CrossRef](#)]
51. Masheder, B.; Urata, C.; Hozumi, A. Transparent and hard zirconia-based hybrid coatings with excellent dynamic/thermoreponsive oleophobicity, thermal durability, and hydrolytic stability. *Appl. Mater. Interfaces* **2013**, *5*, 7899–7905. [[CrossRef](#)] [[PubMed](#)]



© 2017 by the author; licensee MDPI, Basel, Switzerland. This article is an open access article distributed under the terms and conditions of the Creative Commons Attribution (CC-BY) license (<http://creativecommons.org/licenses/by/4.0/>).